

The Novel CPW 2.4 GHz Antenna with Parallel Hybrid Electromagnetic Solar for IoT Energy Harvesting and Wireless Sensors

Irfan Mujahidin^{1*}, Akio Kitagawa²

Micro Electronics Research Laboratory (MeRL), Kanazawa University, Kanazawa, Ishikawa, Japan

Abstract—The design and implementation's novelty simultaneously utilizes the antenna's frequency, polarization, and feed structure to maximize the harvested RF energy and become a microstrip communication circuit for wireless sensor or communication systems in IoT devices. In addition, the optimization of the parallel circuit configuration has a voltage doubler model with an integrated parallel system and thin-film solar cells. Implementation of the antenna structure has two-line feeds in one antenna. Usage both feeds have the same function as CPW circular polarization. Another advantage is that there is no miss-configuration when installing the port exchanges when using both output ports simultaneously. The 2-port antenna has an area of 1/2 per port (where accessible wavelengths work well at the 2.4 GHz frequency). It has been shown to achieve a relatively narrow bandwidth of 86.5 percent covering WiFi frequency band networks and IoT communications. It does not require additional filters and analog matching circuits that cause power loss in the transmission process in parallel voltage doubler circuits. Integrating a reflector on the CPW antenna with two ports for placement of thin-film solar cells provides antenna gain of up to 8.2 dB. It provides a wide beam range with directional radiation. Using a multi-stage parallel to increase voltage output and integrated with a thin-film solar cell converter proves efficient in the 2.4 GHz frequency band. When the transmission power density is -16.15 dBm with a tolerance of 0.023, the novel energy harvester configuration circuit can produce an output voltage of 54 mV dc without adding solar cell energy. And integrated thin-film solar cell a light beam of 300 lux in the radiation beam area of -16.15 dBm, the energy obtained has a value of 1,74467V. It also shows that the implementation of this configuration can produce an optimal dc output voltage in the actual indoor and outdoor ambient settings. The optimization of antenna implementation and the communication process with multiple signal classifications improves the configuration of antennas that are close to each other and have identical phase outputs. It is instrumental and efficient when applied to IoT devices.

Keywords—Double CPW antenna; energy harvesting; wireless sensors; IoT communications

I. INTRODUCTION

Most mobile-based device implementations connect wireless sensor networks, actuators in implementing Internet-of-Things (IoT) communication, manufacturing processes, health care, and transportation. However, the challenges of powering these devices require battery usage, recharging, and power support across multiple sensors. However, it still requires conventional charging, and battery replacement is

becoming very expensive and unsustainable[1][2]. Using energy harvesters to collect energy from environmental sources outside of IoT devices is the most feasible solution. Energy harvesting such as solar, thermal, vibration, piezoelectric, magnetic, and RF are just forms of exploration in collecting energy sources. Film Solar cells with integrated ambient RF or electromagnetic energy collection have better performance than single-source harvesting, based on the principle of using an integrated antenna to harvest energy in the environment and harvesting embedded solar energy indoors or outdoors[3][4]. It can be scaled to multiple nodes either in parallel or partially having high functionality. The technology related to electromagnetic energy harvesting is a wireless power transmission process in which the emitted electromagnetic energy comes from a specific source to be harvested. In addition, the harvesting of electromagnetic energy can be done by collecting sources of electromagnetic radiation present, such as in WLAN systems or other wireless networks, whose use is legally free[5][6]. Harvesting ambient RF energy to support independent IoT devices is becoming practical, increasing devices becoming wireless RF sources.

Most previous research on antennas as electromagnetic energy harvesters only considers partial antenna designs in the one-time harvesting process. They have not utilized antennas as a dual function domain and linear antenna integration. For example, a recent paper presents High-Efficiency Rectenna Broadband for Energy Harvesting RF environment [7]. It only has the function of harvesting single polarized and electromagnetic energy for single antenna use. Consequently, it is essential to use multi-function and optimization of parallel antennas and have directional radiation coverage and power gain to optimize the collection of RF energy in the environment. Antennas with multi-polarization properties can maximize the available RF energy so that absorption from the transmission with random polarization can be well in the IoT device communication system. The configuration has the aim of collecting polarized varying ambient RF energy while minimizing polarization mismatch. It has an alternative to collect ambient RF energy integrated antenna as optimization needs to combine thin-film solar cells [8].

This study proposes a single narrow band electromagnetic environmental energy harvesting device that functions as an electromagnetic energy harvester and wireless sensor[9], especially in IoT devices at the WiFi frequency (2.36-2.44 GHz) integrated with reflectors embedded with The thin-solar cells. Then optimized with parallel configurations to address

*Corresponding Author

the challenges of charging and replacing batteries in IoT devices. Some of our work is: 1) exploiting the antenna function and spatial domain simultaneously, as well as adjusting the polarization to optimize the function as support for sensors or wireless IoT communication and RF energy harvesting, 2) proposing an integrated CPW antenna with a reflector as placement of thin-film solar cells as a canopy on the back of the antenna with the schematic in Fig. 1, 3) provides a design for a compact high gain. To ensure that the dc output voltage can reach 1.2V -1.7V when integrated. [10][4] Provide a comparison of our technology with previous work in outdoor and indoor environments.

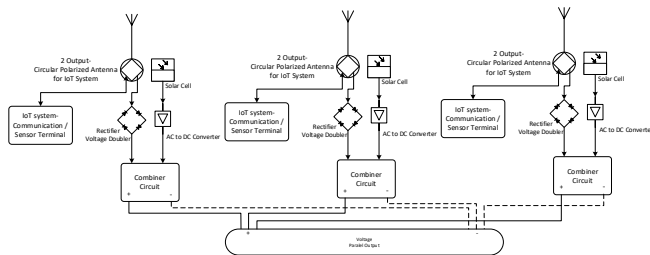


Fig. 1. Schematic of CPW 2.4 GHz Antenna with Parallel Hybrid Electromagnetic Solar for Energy Conversion Systems.

II. PARALLEL HYBRID ELECTROMAGNETIC CIRCUIT

A new 2.4 GHz rectenna was developed and exhibited with optimal configuration dimensions and structures to maximize IoT communication for wireless sensor and voltage. A line of 3 microstrips connects the antenna and the rectifier; Integrating Base Element on FR4 epoxy white paper with a rhombus-shaped slot. Integration is also done on the patch antenna with a radiator in the form of a double patch.

A. Parallel multi Stage Voltage Doubler Parallel Circuit

The rectifier circuit determines the effectiveness of the AC-to-DC Electromagnetic conversion; therefore, this circuit is an essential part of the Hybrid Solar Electromagnetic circuit. The requirements of a suitable rectifier are low power application, high sensitivity, and high voltage handling capability [11]. A rectifier configuration typically consists of an ideal 50-ohm connection for maximum voltage level delivery, a rectifier component (diode) for AC-to-DC Electromagnetic conversion) [12][13]. The only use of power forward in a rectifier circuit is a standard single series diode. The RF power of the antenna is reduced as it passes through the stripline and diode circuits, so direct current is created from the remaining energy.

Due to low power density and unmet circuit bias criteria, single series diode arrays (as opposed to single shunt array diodes) are inefficient for ambient electromagnetic energy collection. In addition, the breakdown voltage of a single diode rectifier is limited, limiting the power handling capacity of the circuit. As a result, as shown in Fig. 2, a rectifier with a voltage multiplier is shown, which implements a modified diode arrangement on a single shunt. The waveform is rectified half-cycle at the positive pole by the diode circuit D1, through the power supply voltage collection at the voltage C1. After the shunt diode D2 rectifies the negative half-cycle of the waveform, the power absorption is at C2. The power voltage C2 can be transferred to C1 in a single series diode arrangement producing a certain energy level around C1 from

an almost simultaneous peak voltage considering the values of RJ, CJ, and Rs on the diode.

As the breakdown voltage of the rectifier increases, the power level of the empirical peak conversion voltage of the rectifier also increases. Furthermore, a partial rectification of the D2 waveform produces a bias voltage of D1 and reduces the input electromagnetic power level (thus increasing the power voltage level sensitivity). The voltage multiplier rectifier was selected for the rectenna design using a bridge type to optimize the voltage output and its architecture in Fig. 4. There are two diodes in each of the two branches.

Some of the results of the previous diode can generate a bias connection of each diode. Use settings that lower the total electromagnetic power consumption. The maximum power level can increase power sensitivity using the half-wave rectifier technique and power level capacity optimization. The choice of the diode is crucial because it can be a significant source of charge voltage and affect circuit performance. Low power input signals (forward bias voltage: 20–100 mV at 0.1 mA) requiring a low bias voltage are ideal for low power applications; diode for parallel selection circuit using Schottky SMS7630.

Another part involved in this circuit is the point of the nonpolar capacitor. The capacitor used in this circuit is a type of Tantalum SMD with a working frequency greater than 2.4 GHz, making it easier to optimize both physically and in terms of calculations. At the same time, optimization [14] on the input impedance of the CMOS circuit chip with a voltage multiplier, where the measurement is challenging and has a reasonably complex stage. To optimize the voltage output in the circuit design, the capacitor on the circuit will cross the load. The output voltage determines the value of the transient response speed for DC leveling.

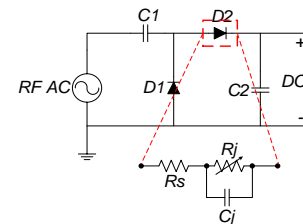


Fig. 2. Voltage Doubler Series on Rectifier.

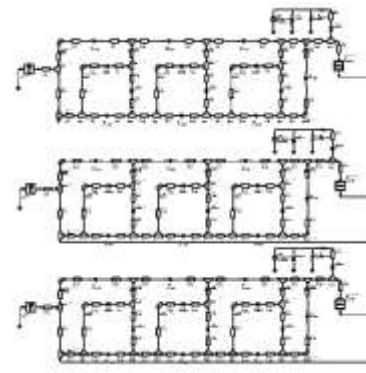


Fig. 3. Simulation using Advanced Design System (ADS) Software.



Fig. 4. Implementation of Rectenna Circuit.

TABLE I. HYBRID ELECTROMAGNETIC SOLAR CIRCUIT - 3 STAGE PARALLEL VOLTAGE DOUBLER STRUCTURE PARAMETERS

No.	Component	Label	Value and Material
1	Non Polar SMD Stage Capacitor	C1, C3, C5, C8, C12, C16, C10, C14, C18	100uF - Tantalum
2		C2, C4, C6, C9, C13, C17, C11, C15, C19	10nF - Tantalum
3	Stage SMD Diode	D1-D19	RB551VM-30
4	Solar Cell Thin Film	hl1	1 mm - Copper
5	Circuit Dimension	Wu,Lu	55.5 mm, 72 mm
6	Copper Conductor	hl2	0.035 mm - Copper
7	Substrate Semiconductor	h	1.6 mm - Phenolic white paper (FR-4)

The most dominant simulation instrument is the Advanced Design System (ADS) software for the configuration and design in Fig. 3. Based on the simulation analysis, the 3-parallel voltage multiplier stage is most suitable for this implementation. For implementing the Rectenna Circuit using the KiCAD software next, the building blocks of printed circuit boards are Basic Epoxy Fiberglass (FR4) (PCB). Table I lists the components in the circuit. Circuit elements consist of active and passive components. Connections to PCBs and other modules using 50 ohm SMA connectors are given special attention because they are related to matching.

B. Microstrip CPW Antenna

Due to the variability of electromagnetic environmental signals, antennas for RF or electromagnetic energy harvesting usually have special requirements. The need for broad direct rays and circularly polarized antennas require an antenna capable of receiving input waves with varying polarization and phase changes. In addition, in antenna performance, it is crucial to consider the quality of the standing wave ratio because hybrid circuits can apply higher working frequency signals and determine conversion at DC voltage levels. The desired frequency band range is 2.3–2.5 GHz. The conventional method for the standing wave ratio is to utilize a bandpass filter between the antennas of a hybrid circuit rectifier to pass another standing wave on a less clear broadband signal in previous studies[15][16]. However, rejecting broadband signals is much more complex than rejecting narrowband signals, so

the proposed antenna uses narrowband. Broadband filters can increase the physical size of the rectenna and large insertion loss voltages [17][18]. As a result, the strategy in this research is to connect a narrowband antenna with a half AC to DC converter integrated with solar cells to get them working frequency focus. The reference antenna (initial setpoint) consists of a planar double pole with two pairs[19]; after optimization and striping the lines, cut square-shaped slots on each pole area to modify the surface, which is 95mm long and 99mm wide.

Furthermore, the second harmonic impedance must be reduced or increased by changing the impedance on the smith chart of the square-shaped slot. The plane of the micro-ground strip antenna, which is orthogonally and behind the microstrip feed line antenna, has two line feeds on it. Ansys HFSS software uses the FEM method to construct microstrip antennas. After calculation and optimization, the high-order parameters are omitted, and the ideal performance of the proposed antenna is shown in Fig. 5.

The partially independent antennae is a narrow band dual-line L feed patch probe antenna, and the 2-port antenna structure is constructed using two antenna elements. Each 2-port antenna configuration has a thin-film solar cell integrated with a reflector to increase gain and optimize radiation. The antenna implementation has microstrip lines printed on the rear, while the 45-degree line feed curve and rectangular cutouts edge are etched on the front. Feed ports 1 and 2 are also shown in Fig. 5. The antenna section comprises a small feed-in with a square cut slot antenna with the exact specifications as a CPW antenna at 2.4 GHz. The length and width of the slot are approximately half a wavelength by design. The optimized ground width in a typical slot mode is a quarter of a wavelength. In optimizing the frequency shift and the patch polarization filter, the slots are optimized into square pieces, and the soil in the area around the square is reduced to a certain extent. The 45-degree line feed antenna works in one wavelength perimeter mode.

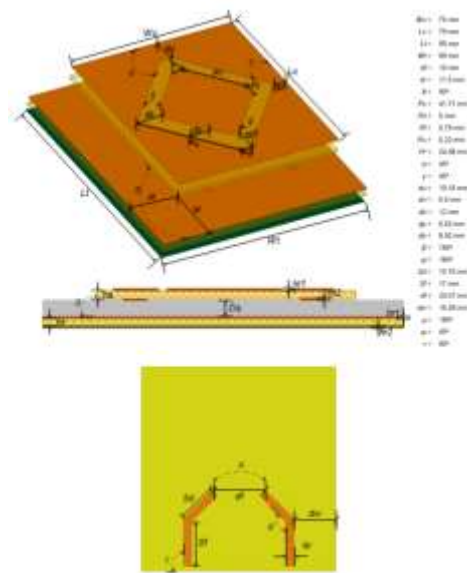


Fig. 5. Structure of Implementation of Double Port CPW Antenna.

To other advantages, the proposed antenna design can adjust the center frequency of the two-port S parameter almost independently under the matching conditions. To tuning it by varying the square side of the ground plane (Prd) in Fig. 6 with length $Prd = Pr-de$, where de is the diagonal edge at the end ground. As illustrated in Fig. 4, the initial simulation of varying $Prd = \{29mm, \dots, 33mm\}$ refers to Fig. 5, while the value of Pr without is adopted for the initial antenna prototype before the optimization.

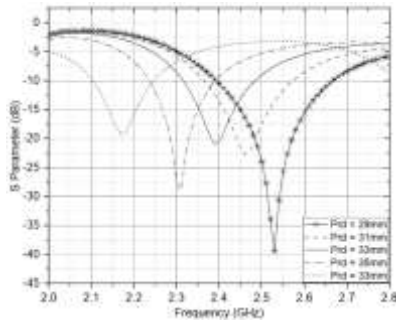


Fig. 6. Tuning Matching Antenna Frequency based on Prd Variation.

However, the frequency adjustment needs to be optimized again by increasing the accuracy of the center value. The optimization with varying dimensions of edge slot on the length square side of the ground. It is interdependent between the horizontal edge Pu and the vertical edge Pt with a symmetrical value resulting from optimizing circular polarization. Figure 5 illustrates with a dimensional accuracy value of up to 0.01mm to obtain frequency accuracy in the variation of dimensions $Pu = \{5.14mm, \dots, 5.26mm\}$ and $Pt = \{5.70, \dots, 5.82\}$, with Pr and Pu values resulting from the final optimization of the antenna, which has been independently combined with other antenna parameters in Fig. 7.

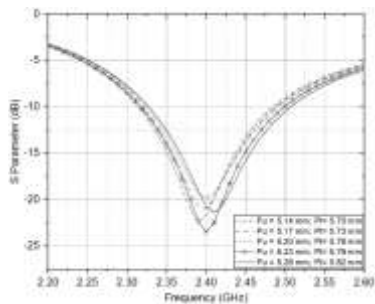


Fig. 7. Increasing the Accuracy of the S parameter Focus Value based on the Edge Ground Dimension Optimization.

The substrate, reflector, and conductor on the patch antenna using a CPW polarized SMA-probe in a narrow band are directly a 1.6 mm thick phenolic patch positioned above the ground and supported by a substrate on a white paper dielectric constant of 4.2. The materials parameters are shown in Table II.

We used a thick air substrate to optimize distance with the integrated thin-film solar cell to increase the radiation gain and beamwidth between the patch and the reflector. The proposed 2-port antenna has an average antenna area of 1:2 per port. It represents a compact multiport antenna design with an open-space wavelength at 2.4 GHz. Therefore, our basis for

calculating the average antenna area per port on the design in free space wavelengths: 1) the primary substrates of the proposed patch antenna are fr4 and antenna; 2) the multiport antenna design is compact, expressing the Freespace wavelength because the nearest antenna port is often connected by air with the requirement with layered material.

TABLE II. MATERIALS STRUCTURE OF THE ANTENNA CONFIGURATION

No.	Parameters	Values	Materials
1	ha	1.6 mm	Copper
2	ht1	0.035 mm	Copper
3	ht2	0.035 mm	Phenolic white paper (FR-4)
4	δ	90°	
5	Ds	5 mm	Air
6	hr	1.6 mm	Copper
7	hr1	0.035 mm	Copper
8	hr2	0.035 mm	Phenolic white paper (FR-4)

III. PERFORMANCE AND ANALYSIS

A. Double port CPW Antenna Performance

Based on measurements, Fig. 8 shows the value of the reflection coefficient with the representation of the S parameter at each port of the antenna. The analysis is carried out first on the narrowband reflection coefficient. The rectangular graph shows a frequency shift between $|S_{11}|$. Measurements and 0.1 GHz range. Port 1 has a bandwidth of -15 dB of 192 MHz (2.353-2.545 GHz), while Port 2 has a -15 dB of 161 MHz (2.36-2.521 GHz) bandwidth. From 2.453 to 2.821 GHz, bandwidth still below -15 dB has a bandwidth of 148 MHz (78 percent) overlap. Overall, the reflection coefficient with the representation of the S parameter value of -15 dB and the spectrum power level test of the antenna can work at a frequency of 2.4GHz, which is shown in Figure 13. The spectrum reception and S Parameters, the antenna based on regulation, can work well for IoT and Energy harvesting applications.

Another performance advantage of the dual-port mode is represented in Fig. 8. Optimizing the microstrip antenna using a reflector integrated with a thin-film solar cell can generate the power gain value in the 2.3–2.5 GHz free IoT communication band with a significant advantage of 8.2 dB at 2.4GHz. The overall gain level is between 8 and 8.6 dB, which is higher than a standard microstrip antenna with an average of 3dB. Optimization of the distance and dimensions of the reflector, which integrates with the thin-film solar cell on the 180-degree position antenna, makes the power signal collection on the radiation element not distorted. Due to the demands of optimal IoT communication, it utilizes circular polarized antennas. It can receive and transmit vertical, horizontal, and other than the two electromagnetic waveforms, so necessary to obtain an axial ratio value below 3dB. Fig. 9 shows the comparison of values between horizontally polarized transmission waves and vertically, expressed by the value of the axial ratio below about 3dB of variation as a representation of circular polarization[16]. Thus the optimization resulting in CPW or total circular polarization is obtained from a symmetrical base

plane with electromagnetic filter effect radiation on the slot on-ground configuration.

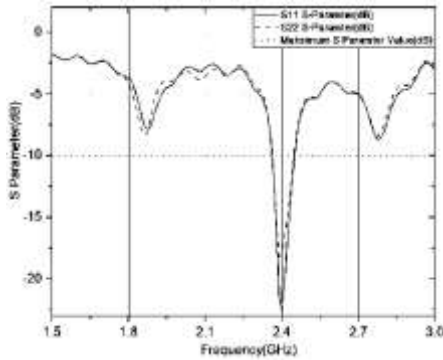


Fig. 8. S Parameters of CPW Dual-Port Microstrip Antenna.

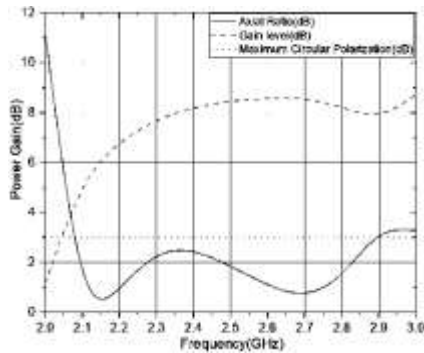


Fig. 9. Gain and Axial Ratio CPW Dual-Port Microstrip Antenna.

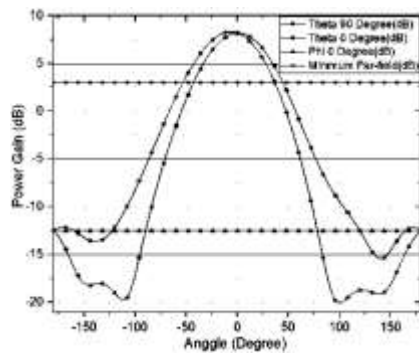


Fig. 10. Radiation Pattern of CPW Dual-Port Microstrip Antenna-Rectangular Plot.

Fig. 10 represents the performance analysis of the antenna implementation based on the typical radiation pattern at an operating frequency of 2.4 GHz inside and on the surface. The performance analysis results match the statistical value of the power distribution level in the direction of the intended device quite well. The radiation pattern is transformed at the position θ with an angle of 90 degrees and θ at 0 degrees. The reference antenna position faces the Z ordinate with a condition of 0 degrees. Hence, Z ordinate radiation the antenna has one lobe with the most significant power level value. It has a minimal sidelobe value on the radiation viewing angle transformation at ϕ on 0 degrees so that the polarization of the Antenna is Directional. To simplify the implementation of the rectenna in the analysis using Fig. 11 using polar coordinates to describe the degree of exposure of the area. The directional

radiation pattern of the antenna indicates that the antenna can be used as an access point in IoT applications to generate energy and communicate directly. The optimization on the square ground plane of the dual-port antenna allows simultaneous vertical and horizontal polarization. The proposed antenna has the following advantages: small overall size, optimal bandwidth, and not cross-polarization.

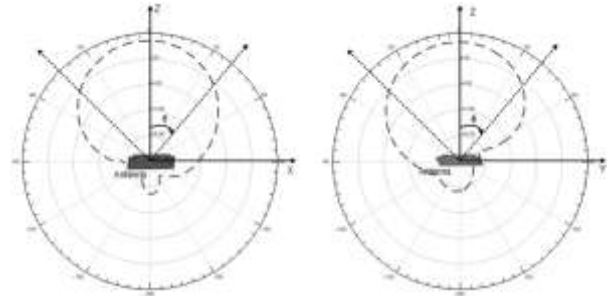


Fig. 11. Radiation Pattern CPW Dual-Port Microstrip Antenna-Polar Plot.

B. Performance Electromagnetic-Solar with Parallel CPW antenna Circuit Integrated

In the parallel circuit performance test, the receiving antenna is connected to the rectifier circuit via an SMA connection with a characteristic impedance of 50 ohms. The produced rectenna was tested in the laboratory, as illustrated in Fig. 12. The performance of the rectifier circuit as determined by the AC-DC voltage conversion value and the output frequency is illustrated in Fig. 13 and 14, respectively, used the same experimental data collection technique with different configurations of performance measurements as in Fig. 12(b).

The rectifier circuit, Receiver antenna, and thin film can be directly connected because the dual output feed antenna and the input port of the rectifier circuit have the same impedance as the output port. In addition, the circuit configuration has a compact implementation for other ports as the IoT communication feed line. However, to make measurements more movable in the laboratory using a coaxial cable with an adjustable impedance. The results of the performance measurements of the rectenna are in Fig. 12(b). a signal generator connected to the SHRP RZ1AT4A antenna as a microstrip antenna used in industry is the signal source to spread electromagnetic waves in the laboratory area. Then the antenna absorption value is expressed by testing the spectrum in Fig. 13, which works well at a frequency of 2.4 GHz, which consists of -16.15 dBm, -23.66 dBm, and -33.89 dBm, because testing the signal spectrum is also very important when used in the communication process on IoT devices.

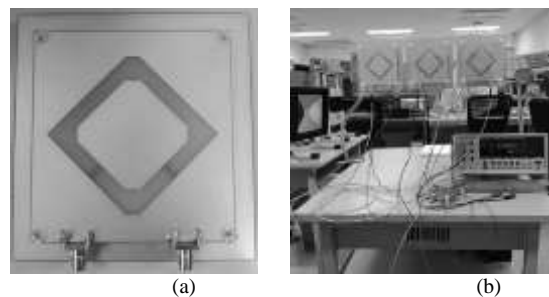


Fig. 12. (a) Antenna Implementation and (b) Configuration Circuit Testing.

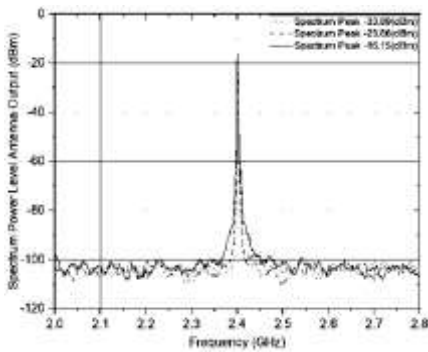


Fig. 13. Antenna Spectrum Test at a Frequency of 2.4 GHz.

The absorbed energy is amplified using a voltage doubler with a parallel and simultaneous configuration with a maximum absorption rate of -16.15 dBm antenna and a frequency range of 2.0 GHz to 2.8 GHz. At the primary working frequency of 2.4 GHz, the transmitting antenna is a beam with a power level of 20 dB.

At the input power of -16.15 dBm, the output voltage with an electromagnetic field source in the single rectenna circuit configuration with 3 stage doubler has a value of 29.3 mV. The parallel circuit configuration has a value of 52 mV, as shown in Fig. 14. Fig. 14 shows that the increase is quite significant if the configuration is optimized to be parallel with the analysis of equation 1, which shows an efficient circuit performance, where the value of R_{iL} is the value of the resistance of the circuit. $V_{Pcircuit}$ is the output voltage of the rectifier circuit, R_0 is the internal resistance of the transmission medium, μ is the characteristic coefficient of the circuit voltage quantity with a value of 0.6, and n_p is the number of parallel lines sources in the circuit.

$$V_{Pcircuit} = \mu n_p \frac{n_0 V_0}{n_0 R_0 + R_{iL}} R_{iL} \quad (1)$$

Fig. 16 shows the performance of the Parallel 3 Stage Voltage Doubler Circuit. It generates an output voltage and AC voltage conversion from the rectenna with variations in the power level collected at the same value on two 2.4GHz ports based on the variable transmit power source, namely, the RF source and light intensity. First, the circuit performance test is comprehensively tested with various light conditions in Fig. 15.

When the light intensity received by the thin-film solar cell increases, the output voltage increases whether used in single or parallel configurations. The output voltage in the configuration proposed in this study, a parallel configuration with the integration of thin-film solar cells, has an output voltage of 1.74467V with a light-emitting source of 300 lux in Fig. 16. The parallel circuit has the advantage of increasing the voltage up to 80% compared with a single [20] configuration. In addition, integration with solar cells can also increase the power up to 25 times if only relying on electromagnetic sources [21]. In this case, the electromagnetic source is inferior, according to the source in the IoT device.

The optimization of the design and implementation significantly improves compared to previous studies [22][10]. This Reference only relied on a single configuration and one

particular application. The increase in the voltage value in the circuit test on the independent variable shows that it can work well, both from one energy source and two sources of energy.

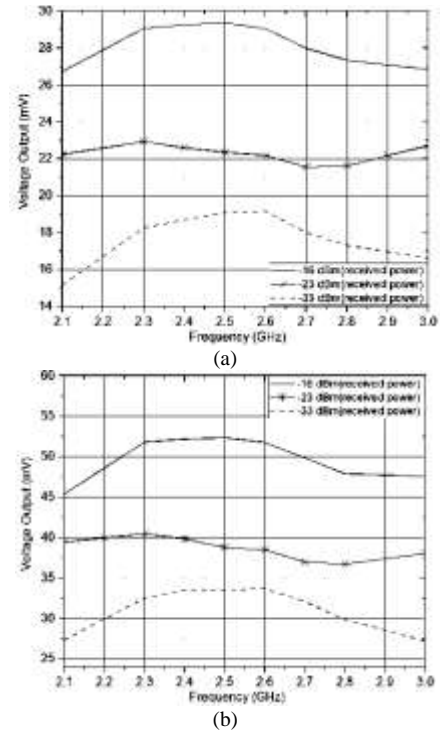


Fig. 14. Antenna Output Voltage in an (a) Single and (b) Parallel Three-Stage-Voltage Doubler Circuit.

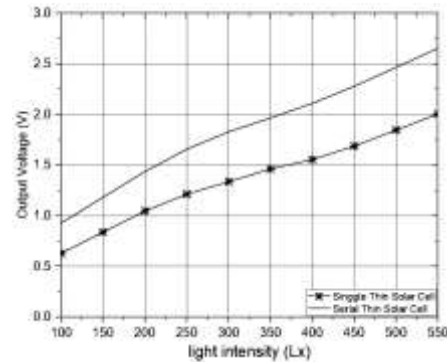


Fig. 15. AC to DC Conversion Test on Solar Cell Film.

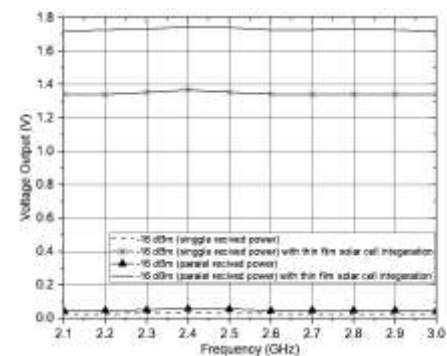


Fig. 16. Performance of Integrated Parallel Rectenna-thin Film Solar Cell Output Voltage.

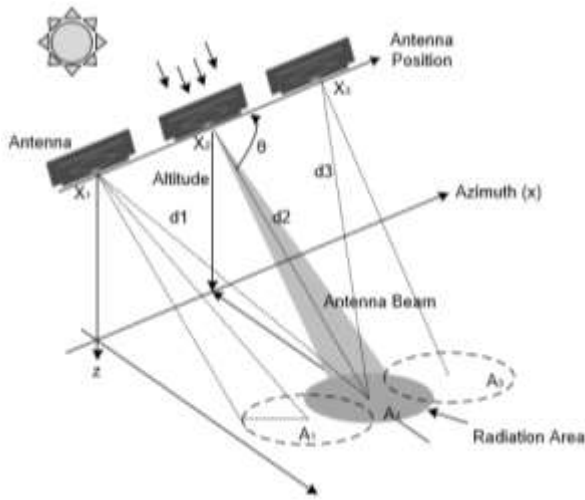


Fig. 17. Overall Implementation Analysis of the Integrated Rectenna-thin Film Solar Cell Prototype.

Fig. 17 shows the overall implementation analysis scheme of the prototype that has been tested in the laboratory. Implementing energy harvesting with the integration of thin-film solar cells is estimated as exposure to sunlight, 100 lux when cloudy to 1000 lux maximum. This range is following the performance test of the lowest voltage limit on the prototype for implementation. In addition, the implementation of the energy harvesting and communication process must adjust the radiation angle based on Fig. 10 and 11 of the antenna element radiation patterns. The optimum main lobe value at the antenna altitude is θ of 48 degrees, with overlapping antenna beam coverage areas. However, the antenna has almost the same phase in IoT communication and has a close position [23]. Therefore, it is necessary to analyze the signal with high accuracy to determine the number and direction of arrival of the antenna signal by using multiple signal classification analysis for Linear Array elements assuming the antenna's position with the number of transmitting sample signals analysis 1000 times and four source antennas, one antenna as a reference. Azimuth antenna on identical antenna elements based on Fig. 5, then the array manifold $a(\theta)$ is determined:

$$a(\theta) = \begin{bmatrix} 1 \\ e^{j2\pi d_1 \sin\theta_1/0.0125} \\ e^{j2\pi d_2 \sin\theta_2/0.0125} \\ e^{j2\pi d_3 \sin\theta_3/0.0125} \end{bmatrix}$$

Where d is the distance from a common reference point in the array and the azimuth coordinate antenna θ that the direction measured from the perpendicular to the array, so if applied to multiple antennas with the transmission on communication devices with F is the amplitude at the 2.4GHz frequency of the antenna devices.

$$\begin{bmatrix} X_1 \\ X_2 \\ X_3 \\ X_4 \end{bmatrix} = [a(\theta_1) \ a(\theta_2) \ a(\theta_3) \ a(\theta_4)] \begin{bmatrix} F_1 e^{j15.085 \times 10^9 t} \\ F_2 e^{j15.085 \times 10^9 t} \\ F_3 e^{j15.085 \times 10^9 t} \\ F_4 e^{j15.085 \times 10^9 t} \end{bmatrix}$$

Signal transmit of device source with random amplitude on covariance matrix:

$$s = \begin{bmatrix} -0.2523 - 4.0111i & -3.0320 + 0.3830i & \dots & -1.3591 + 2.3441e - 13i \\ 0.4964 + 7.8909i & 2.6104 - 0.3297i & \dots & 0.4605 - 7.9429e - 14i \\ -0.2283 - 3.6299i & 1.6989 - 0.2146i & \dots & 1.9914 - 3.4346e - 13i \\ -0.4224 - 6.7140i & 2.4543 - 0.3100i & \dots & 2.1928 - 3.7827e - 13i \end{bmatrix}$$

With resultant steering vector between incoming signals $F_1 e^{j15.085 \times 10^9 t}$ and A is steering matrix $a(\theta)$, then $a(\theta)$ is $\chi = A \times s$ dan $\overline{\chi \chi^*}$ ensemble average so $\overline{\chi_1 \chi_1^*}, \overline{\chi_2 \chi_2^*}, \overline{\chi_3 \chi_3^*}, \overline{\chi_4 \chi_4^*}$ Autocorrelation with the R_{ss} . Then R_{ss} autocorrelation input signal itself and the other cross-correlation value on the signal on the assumption of the signal plane then the covariance matrix for the incoming signal:

$$\overline{\chi \chi^*} = \begin{bmatrix} \overline{\chi_1 \chi_1^*} & \overline{\chi_1 \chi_2^*} & \overline{\chi_1 \chi_3^*} & \overline{\chi_1 \chi_4^*} \\ \overline{\chi_2 \chi_1^*} & \overline{\chi_2 \chi_2^*} & \overline{\chi_2 \chi_3^*} & \overline{\chi_2 \chi_4^*} \\ \overline{\chi_3 \chi_1^*} & \overline{\chi_3 \chi_2^*} & \overline{\chi_3 \chi_3^*} & \overline{\chi_3 \chi_4^*} \\ \overline{\chi_4 \chi_1^*} & \overline{\chi_4 \chi_2^*} & \overline{\chi_4 \chi_3^*} & \overline{\chi_4 \chi_4^*} \end{bmatrix} = A R_{ss} A^* + \text{power noise}$$

Then, extract the signal information using the Eigenvector of $A R_{ss} A^*$ and the Eigenvector of noise power to generate the signal eigenvalues and the noise eigenvalues. We can describe the value noise subspace from the D matrix for the eigenvalue.

$$D = \begin{bmatrix} 8.8141e - 05 & 0 & 0 & 0 & 0 \\ 0 & 9.7605e - 05 & 0 & 0 & 0 \\ 0 & 0 & 1.010e - 04 & 0 & 0 \\ 0 & 0 & 0 & \ddots & 0 \\ 0 & 0 & 0 & 0 & 1.4814 \end{bmatrix} \approx \begin{bmatrix} 1 & 0 & 0 & 0 & 0 \\ 0 & 1 & 0 & 0 & 0 \\ 0 & 0 & 1 & 0 & 0 \\ 0 & 0 & 0 & \ddots & 0 \\ 0 & 0 & 0 & \dots & 1 \end{bmatrix}$$

Then describe each Rank on the signal eigenvalues and eigen noise = E_i to determine the trash hold value of the signal. From this treatment, we can obtain a spectrum picture of each signal using the multiple signal classification equations 2.

$$P = \frac{1}{a^*(\theta) \cdot E_i \cdot E_i^* \cdot a(\theta)} \quad (2)$$

The spectrum generated can be analyzed of each incoming signal spectrum result and the angle of origin signal even though the phase is almost identical, and the position is close to each other seen in Fig. 18. The spectrum shows a signal from the antenna with a directional arrival angle of $1/\text{Norm}^2$ on each power signal. Information appears at 61, 92, 125, and 180 degrees for the analysis sample. Thus, the analysis can provide an efficient solution to the proposed configuration using a liner position antenna with circular antenna specifications when working as an IoT communication for wireless sensors antenna and energy harvester.

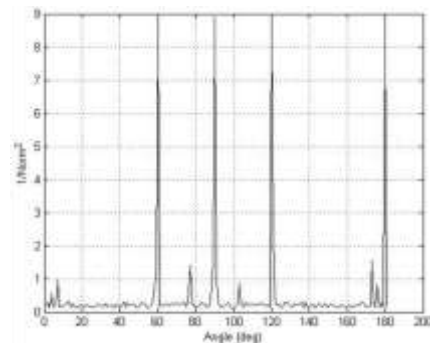


Fig. 18. Spectrum Analysis of Incoming Signals on Multiple Antennas.

IV. CONCLUSION

This article is based on performance tests and a new analysis of IoT Energy Harvesting and Wireless Sensors using 2.4 GHz CPW Antenna with Parallel Hybrid Electromagnetic Solar. A 2.4 GHz CPW rectangular dual-port antenna with IoT Wearable broadband, direction power beamwidth, and high gain is used as the receiving antenna. The proposed configuration includes a 2.4 GHz CPW rectangular dual-port antenna rectifier circuit based on IoT communication and the concept of parallel voltage doubling with an integrated thin-film solar cell. The performance of the microstrip antenna input and output of the S parameters of network feed with S11 -18.02 and dB S21 -24.7 dB, gain value of 11dbi, and axial ratio value of 2.46. According to these tests, the configuration of the rectifier and antenna circuits has a very narrow operating frequency range. And can be used effectively in any direction based on the radiation polarization. In addition, the integrated Rectenna has a compact design and is easy to apply. In the energy harvester performance test at the input power of -16.15 dBm, the output voltage with an electromagnetic field source, the single rectenna circuit configuration with 3 stage doublers has a value of 29.3 mV, and the parallel circuit configuration has a value of 52 mV. In addition, the output voltage in the configuration proposed in this study, which is a parallel configuration with the integration of thin-film solar cells, has an output voltage of 1.74467V. This configuration has the advantage of increasing the voltage up to 80% compared to the single configuration. In addition, integration with solar cells can also increase the temperature up to 25 times if only relying on electromagnetic sources. Based on the implementation analysis, the configuration energy harvester with thin-film solar cell integration can work up to at least 100 lux exposures to sunlight. And the electromagnetic transmission area will work optimally at an angle of 48 degrees based on the radiation pattern, and the prototype of IoT communication analysis can be implemented. Multiple signal classification for Linear Array for circular polarization antenna with high accuracy to determine the spectrum of each incoming signal and the angle of origin of the signal even with almost the identical phase. In progress, the development of this prototype is to become more compact and work on the working frequency of other IoT devices so that there are more options to be implemented.

REFERENCES

- [1] Naresh, V. K. Singh, and V. K. Sharma, "Integration of microstrip patch antenna with flexible thin film solar cell," *Int. J. Innov. Technol. Explor. Eng.*, vol. 8, no. 11, 2019, doi: 10.35940/ijitee.K1544.0881119.
- [2] R. Yuwono, I. Mujahidin, A. Mustofa, and Aisah, "Rectifier using UFO microstrip antenna as electromagnetic energy harvester," *Adv. Sci. Lett.*, vol. 21, no. 11, 2015, doi: 10.1166/asl.2015.6574.
- [3] S. Kim, M. M. Tentzeris, and A. Georgiadis, "Hybrid printed energy harvesting technology for self-sustainable autonomous sensor application," *Sensors (Switzerland)*, vol. 19, no. 3, 2019, doi: 10.3390/s19030728.
- [4] R. Yuwono and I. Mujahidin, "Rectifier using UWB microstrip antenna as electromagnetic energy harvester for GSM, CCTV and WiFi transmitter," *J. Commun.*, vol. 14, no. 11, 2019, doi: 10.12720/jcm.14.11.1098-1103.
- [5] D. A. Prasetya and I. Mujahidin, "2.4 GHz Double Loop Antenna with Hybrid Branch-Line 90-Degree Coupler for Widespread Wireless Sensor," 2020, doi: 10.1109/EECCIS49483.2020.9263477.
- [6] E. Sonalitha, B. Nurdewanto, A. Zubair, S. R. Asriningtias, K. Yudhistiro, and I. Mujahidin, "Blackbox Testing Model Boundary Value of Mapping Taxonomy Applications and Data Analysis of Art and Artworks," 2020, doi: 10.1109/ISRITI51436.2020.9315406.
- [7] Y. Shi, Y. Fan, Y. Li, L. Yang, and M. Wang, "An efficient broadband slotted rectenna for wireless power transfer at LTE band," *IEEE Trans. Antennas Propag.*, vol. 67, no. 2, 2019, doi: 10.1109/TAP.2018.2882632.
- [8] E. V. V. Cambero, H. P. Da Paz, V. S. Da Silva, H. X. De Araujo, I. R. S. Casella, and C. E. Capovilla, "A 2.4 GHz Rectenna Based on a Solar Cell Antenna Array," *IEEE Antennas Wirel. Propag. Lett.*, vol. 18, no. 12, 2019, doi: 10.1109/LAWP.2019.2950178.
- [9] U. Dudko and L. Overmeyer, "Optical Wake-Up from Power-Off State for Autonomous Sensor Nodes," *IEEE Sens. J.*, vol. 21, no. 3, 2021, doi: 10.1109/JSEN.2020.3023817.
- [10] J. Bito, R. Bahr, J. G. Hester, S. A. Nauroze, A. Georgiadis, and M. M. Tentzeris, "A Novel Solar and Electromagnetic Energy Harvesting System with a 3-D Printed Package for Energy Efficient Internet-of-Things Wireless Sensors," *IEEE Trans. Microw. Theory Tech.*, vol. 65, no. 5, 2017, doi: 10.1109/TMTT.2017.2660487.
- [11] M. Son, A. Pinnola, R. Bassi, and G. S. Schlau-Cohen, "The Electronic Structure of Lutein 2 Is Optimized for Light Harvesting in Plants," *Chem*, vol. 5, no. 3, 2019, doi: 10.1016/j.chempr.2018.12.016.
- [12] K. K. A. Devi, N. M. Din, and C. K. Chakrabarty, "Optimization of the Voltage Doubler Stages in an RF-DC Converter Module for Energy Harvesting," *Circuits Syst.*, vol. 03, no. 03, 2012, doi: 10.4236/cs.2012.33030.
- [13] E. Sonalitha et al., "Combined text mining: Fuzzy clustering for opinion mining on the traditional culture arts work," *Int. J. Adv. Comput. Sci. Appl.*, vol. 11, no. 8, 2020, doi: 10.14569/IJACSA.2020.0110838.
- [14] A. Y. S. Jou, R. Azadegan, and S. Mohammadi, "High-Resistivity CMOS SOI Rectenna for Implantable Applications," *IEEE Microw. Wirel. Components Lett.*, vol. 27, no. 9, 2017, doi: 10.1109/LMWC.2017.2734776.
- [15] Y. Li, Z. Zhao, Z. Tang, and Y. Yin, "Differentially Fed, Dual-Band Dual-Polarized Filtering Antenna with High Selectivity for 5G Sub-6 GHz Base Station Applications," *IEEE Trans. Antennas Propag.*, vol. 68, no. 4, 2020, doi: 10.1109/TAP.2019.2957720.
- [16] I. Mujahidin, D. A. Prasetya, A. B. Setywan, and P. S. Arinda, "Circular Polarization 5.5 GHz Double Square Margin Antenna in the Metal Framed Smartphone for SIL Wireless Sensor," 2019, doi: 10.1109/ISITIA.2019.8937257.
- [17] Z. Zheng, X. Fang, W. Wang, G. Huang, H. Zhang, and X. Liang, "A Compact Waveguide Slot Filtering Antenna Based on Mushroom-Type Surface," *IEEE Antennas Wirel. Propag. Lett.*, vol. 19, no. 10, 2020, doi: 10.1109/LAWP.2020.3020539.
- [18] I. Mujahidin, S. H. Pramono, and A. Muslim, "5.5 GHz Directional Antenna with 90 Degree Phase Difference Output," 2018, doi: 10.1109/EECCIS.2018.8692872.
- [19] I. Mujahidin, D. A. Prasetya, Nachrowie, S. A. Sena, and P. S. Arinda, "Performance tuning of spade card antenna using mean average loss of backpropagation neural network," *Int. J. Adv. Comput. Sci. Appl.*, no. 2, 2020, doi: 10.14569/ijacsa.2020.0110280.
- [20] Z. He, H. Lin, and C. Liu, "Codesign of a Schottky Diode's and Loop Antenna's Impedances for Dual-Band Wireless Power Transmission," *IEEE Antennas Wirel. Propag. Lett.*, vol. 19, no. 10, 2020, doi: 10.1109/LAWP.2020.3019739.
- [21] H. Zhang and T. Ngo, "Linear-Polarization-Insensitive Rectenna Design for Ground-to-Air Microwave Power Transmission," *IEEE Access*, vol. 8, 2020, doi: 10.1109/ACCESS.2020.2998182.
- [22] A. I. Imran, T. A. Elwi, and A. J. Salim, "On the distortionless of uwb wearable hiltbert-shaped metamaterial antenna for low energy applications," *Prog. Electromagn. Res. M*, vol. 101, 2021, doi: 10.2528/PIERM20113008.
- [23] G. K. Kurt et al., "A Vision and Framework for the High Altitude Platform Station (HAPS) Networks of the Future," *IEEE Commun. Surv. Tutorials*, vol. 23, no. 2, 2021, doi: 10.1109/COMST.2021.3066905.